The Journal of Cardiovascular Surgery 2022 August;63(4):454-63
DOI: 10.23736/S0021-9509.22.11980-4

ORIGINAL ARTICLE
VASCULAR SECTION

Evaluation of electrocardiogram-gated computed tomography angiography to quantify changes in geometry and dynamic behavior of the iliac artery after placement of the Gore Excluder Iliac Branch Endoprosthesis

Majorie van HELVERT [1, 2], Jaimy A. SIMMERING [1, 3] *, Maaike A. KOENRADES [1, 4], Cornelis H. SLUMP [5], Jan M. HEYLIGERS [6], Robert H. GEELKERKEN [1, 3], Michel M. REIJNEN [1, 2]

[1]Multi-Modality Medical Imaging Group, TechMed Centre, University of Twente, Enschede, the Netherlands; [2]Department of Vascular Surgery, Rijnstate Hospital, Arnhem, the Netherlands; [3]Department of Vascular Surgery, Medisch Spectrum Twente, Enschede, the Netherlands; [4]Department of Medical Technology, Medical 3D lab, Medisch spectrum Twente, Enschede, the Netherlands; [5]Robotics and Mechatronics Group, TechMed Centre, University of Twente, Enschede, the Netherlands; [6]Department of Vascular Surgery, Elisabeth-TweeSteden Hospital, Tilburg, the Netherlands

*Corresponding author: Jaimy A. Simmering, Multi-Modality Medical Imaging Group, TechMed Centre, University of Twente, P.O. Box 217, 7500 AE Enschede, the Netherlands. E-mail: j.a.simmering@utwente.nl

ABSTRACT

BACKGROUND: The GORE® EXCLUDER® Iliac Branch Endoprosthesis (IBE) is designed to treat iliac aneurysms with preservation of blood flow through the internal iliac artery (IIA). Little is known about the influence of IBE placement on the IIA geometry. This study aimed to provide detailed insights in the dynamic behavior and geometry of the common iliac artery (CIA) and IIA trajectory and how these are influenced after treatment with an IBE.

METHODS: Pre- and postoperative electrocardiogram-gated computed tomography angiography (ECG-gated CTA) scans were acquired in a prospective study design and analyzed with in-house written algorithms designed for aorto-iliac and endoprosthesis deformation evaluation. Cardiac pulsatility-induced motion patterns and pathlengths were computed by tracking predefined locations on the aorto-iliac tract. Centerlines through the CIA-IIA trajectory were used to investigate the static and dynamic geometry, including curvature, torsion, length and Tortuosity Index (TI).

RESULTS: Fourteen CIA-IIA trajectories were analyzed before and after IBE placement. Cardiac pulsatility-induced motion and pathlengths increased after IBE placement, especially at mid IIA and the first IIA bifurcation ($P \leq 0.04$). After IBE placement, static and dynamic curvature, length and TI decreased significantly ($P<0.05$). Furthermore, the average dynamic torsion increased significantly ($P=0.030$). The remaining geometrical outcomes were not statistically significant.

CONCLUSIONS: The placement of an IBE device stiffens and straightens the CIA-IIA trajectory. Its relation with clinical outcome is yet to be investigated, which can be done thoroughly with the ECG-gated CTA algorithms used in this study.

(*Cite this article as*: van Helvert M, Simmering JA, Koenrades MA, Slump CH, Heyligers JM, Geelkerken RH, *et al.* Evaluation of electrocardiogram-gated computed tomography angiography to quantify changes in geometry and dynamic behavior of the iliac artery after placement of the Gore Excluder Iliac Branch Endoprosthesis. J Cardiovasc Surg 2022;63:454-63. DOI: 10.23736/S0021-9509.22.11980-4)

KEY WORDS: Iliac aneurysm; Blood vessels; Computed tomography angiography.

The presence of a concomitant aneurysm of the common iliac artery (CIA), found in 20-40% of the patients with an abdominal aorta aneurysm patients, challenges standard endovascular aneurysm repair (EVAR) due to an insufficient distal sealing zone.[1, 2] The use of bell-bottom limbs is a valid option for concomitant CIA aneurysms with a diameter ≤24-25 mm, but is related to more complications during follow-up.[3] Exclusion of the CIA aneurysm by covering the internal iliac artery (IIA), with or without IIA embolization, is considered a safe alternative.[4] However, this strategy is related to ischemic complications, including invalidating buttock claudication (16-55%), erectile dysfunction (10-46%) and rarely spinal cord and colonic ischemia (<1%).[5, 6] To preserve pelvic circulation, and thus to reduce the incidence of pelvic ischemic complications, iliac branched devices were developed.[6] One of these is the Iliac Branch Endoprosthesis (IBE) of the *GORE*® EXCLUDER® platform (W.L. Gore & Associates, Flagstaff, AZ, USA), which consists of an iliac branch component and a self-expanding IIA component of equal structure and composition. Short- and midterm results of the IBE are encouraging, with primary technical success rates of 94-100%,[7-10] primary IIA patency rates of 90-95% at 6 months[7-10] and 93.6% at both 12 and 24 months[11] and overall freedom-from-reintervention rates of 95-100% at 6 months[7-10] and 90.4% at 24 months,[11] respectively. Long-term results of the IBE are still awaited.

In general, the implantation of an endoprosthesis causes a straightening of the aorto-iliac axis, especially in case of strong tortuosity of the native vessels.[12] Advanced aorto-iliac aneurysmal disease is reflected in both an increased perirenal α- or β-angle and iliac tortuosity, which apply stresses to the endoprosthesis that may lead to complications, such as type Ia, Ib or III endoleaks, kinking and endoprosthesis thrombosis.[13-16] Taudorf *et al.* showed a relation between the tortuosity of a vessel and the risk of limb occlusion in regular EVAR.[14] Since the iliac arteries can exhibit severe tortuosity, iliac branched devices are subjected to higher tortuosity constraints than regular EVAR devices. Thus far, only one study investigated the static geometrical changes of the iliac arteries after IBE implantation.[17] Albeit an IBE is placed to preserve flow through the IIA, the influence on the dynamic behavior and geometry of the IIA remains unknown. Dynamic behavior, *i.e.* cardiac pulsatility-induced motion and geometrical changes, can be analyzed using electrocardiogram (ECG)-gated computed tomography angiography (CTA) scans. These type of analysis have provided useful insights for other endoprostheses.[16, 18-23]

The aim of this study was to quantify dynamic behavior and geometry of the CIA-IIA trajectory before and six weeks after implantation of an IBE, using dedicated analysis algorithms on ECG-gated CTA. This may lead to a better understanding of dynamic and geometrical behavior of IBE devices and provide insight into the mechanisms of underlying potential endoprosthesis failure. Ultimately, this may aid to further improvement of future devices and procedural planning.

Materials and methods

Study design and population

Between July 2017 and April 2020 fifteen patients scheduled for implantation of an IBE device were prospectively enrolled in this exploratory two-centered study. Procedures were performed according to the hospital's standard practice. After IBE placement, patients received dual antiplatelet therapy for six months followed by single antiplatelet therapy. Procedural details and further device descriptions of the IBE have been described previously.[7] ECG-gated CTA scans were acquired prior to and six weeks after the procedure as substitute for the routine CTA scans. Approval was obtained from the ethical committee and the institutional review boards. The trial was registered on ClinicalTrials.gov (NCT03762525). All patients provided written informed consent before participation. No exclusion criteria were defined.

Image acquisition

All ECG-gated CTA scans were performed on a 256-slice CT scanner (Brilliance iCT 256; Philips Healthcare, Best, the Netherlands) with a standardized arterial scan protocol. Scan parameters were as follows: tube voltage, 100-120 kV; tube current time product, 205-956 mA·s; collimation, 80x0.625 mm; rotation time, 0.27-0.33 s; slice thickness, 0.8-0.9 mm; slice increment, 0.4-0.7 mm; reconstruction matrix, 512×512 pixels; pitch factor, 0.18-0.30. A total of 100 mL of radiocontrast agent (Xenetix 350) was intravenously administered at 5 mL/s, without medical premedication. The scans were obtained during a single inspiration breath hold after performing a standard breathing exercise. Retrospective gating was applied to obtain 10 equally binned phases of the cardiac cycle from 0% to 90% of the RR interval.

Image processing

Image processing was conducted in Python programming language (version 3.7) using a previously established combined image registration and segmentation algorithm.[24-26]

The processing steps include registration of the 3D volumes of all 10 phases to obtain a motion compensated, 3D volume (*i.e.* static, mid cardiac cycle, CT volume) and 10 deformation fields describing the displacement of each voxel in an individual phase with respect to mid cardiac cycle.

Motion patterns

To quantify the cardiac pulsatility-induced motion of the native and stented iliac anatomy in *x*-, *y*- and *z*-direction, a set of points was manually selected in the pre- and postoperative static CT volume. In the preoperative scan, points were selected on the following anatomical structures: the native aorta bifurcation, CIA bifurcation, halfway between the origin and the first bifurcation of the IIA, and the first IIA bifurcation (Figure 1A). In the postoperative scan, these points were represented by the bifurcation of the main endoprosthesis, the IBE flow divider, the distal markers of the IIA component, and the first IIA bifurcation (Figure 1B). It should be noted that, although in close proximity, the selected points differ slightly between pre- and postoperative scans. However, they do resemble the same anatomical locations, including new (endograft) bifurcations at which similar hemodynamic forces are expected to be exerted. For all selected points, the motion in *x*-, *y*- and *z*-direction for each phase of the cardiac cycle was automatically obtained by applying the deformation fields through backward mapping. Also, the sum of displacement for each individual landmark during the cardiac cycle, hereafter pathlength, was obtained. The inter- and intra-observer variability were determined by additional point selection in all patients by the initial and a second observer.

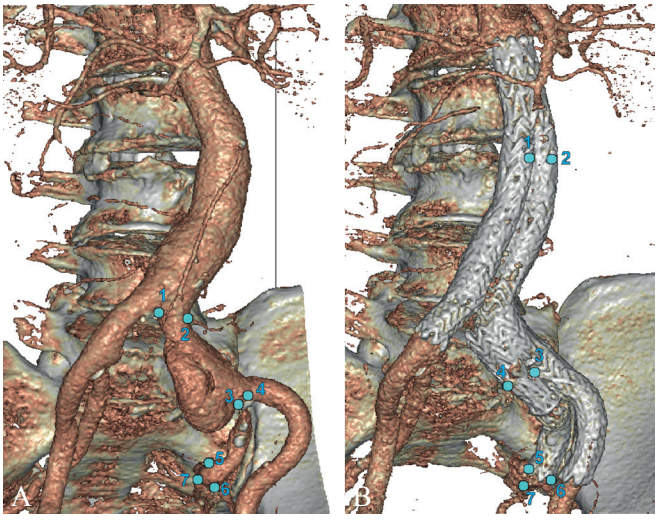

Figure 1.—3D volume representation of a patient before (A) and after (B) treatment with an iliac branch endoprosthesis (IBE). The selected points are presented in blue in the online version. The corresponding landmarks are: 1 and 2: aorta bifurcation/flow divider main device; 3 and 4: common iliac artery bifurcation/flow divider IBE; 5 and 6: mid internal iliac artery (IIA)/distal marker of IIA component, 7; IIA bifurcation distal to the IBE.

Geometrical changes

The aorto-iliac tract and endoprosthesis were segmented using the static CT volume with a thresholding operation of respectively 150-350 and 500-650 Hounsfield units. Subsequently, centerlines of the vasculature were obtained as detailed elsewhere.[16, 18] Postoperatively, start and end of the centerline were defined at the origin of the CIA and the first bifurcation of the IIA, respectively. By referencing anatomical landmarks, similar start and end were selected in the preoperative CTA scan, making the obtained pre- and postoperative centerline comparable for analysis. Each centerline consisted of a number of points at a set distance of 1 mm. This centerline served as a basis for the subsequent static geometry analysis. The course of the centerline at each phase of the cardiac cycle was obtained after backward-mapping by applying the deformation fields. These centerlines were used for subsequent dynamic geometry analysis.

Curvature is used to describe the bending of the vessel centerline and was calculated for each centerline point.[16] Torsion describes to what extent the centerline twists out of the plane of the curvature for each centerline point.[27] First, curvature and torsion were calculated for each point on the static centerline. The average and maximum static curvature and torsion were computed by taking the average and maximum of all values. Next, curvature and torsion were calculated for each point on the dynamic centerlines, resulting in 10 values per point. The difference between the smallest and largest value per point was defined as the dynamic value. Subsequently, the average and maximum dynamic curvature and torsion were obtained by taking the average and maximum of all dynamic values. Initially torsion values can be either positive or negative, indicating the direction of twisting. To avoid disregarding of negative values when computing the maximum static or dynamic torsion, the absolute value was taken. In addition, the location of maximum static and dynamic curvature and were categorized based on visual inspection of color-coded centerlines (Figure 2).

The length of the centerline was calculated as the sum of all individual distances between consecutive points on the centerline. The Tortuosity Index (TI) was defined as the length of the centerline divided by the straight distance be-

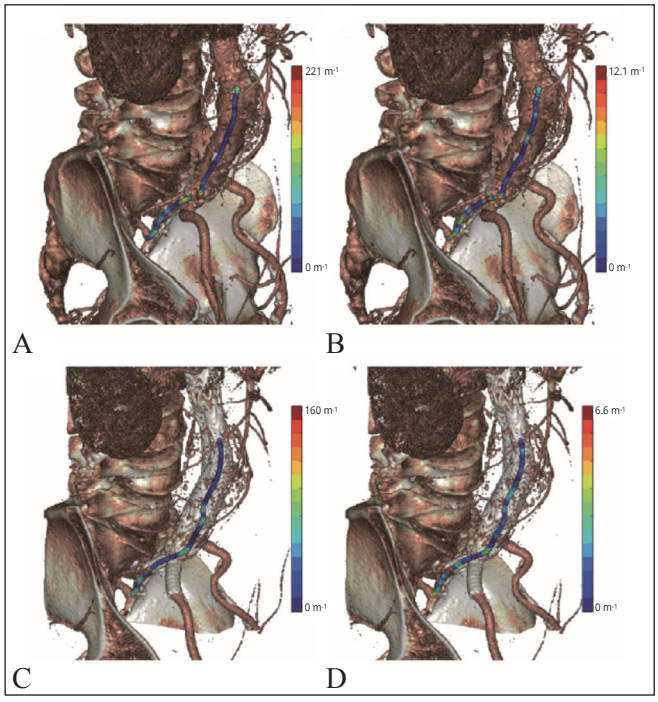

Figure 2.—Color-coded centerlines superimposed on a 3D volume representation of a patient. Color in the online version indicates static and dynamic curvature before (A and B, respectively) and after (C and D, respectively) treatment. Note the difference in maximum curvature per color bar.

tween start and end of the centerline. Dynamic length and TI were defined as the difference between the minimum and maximum value of length and TI over the 10 phases.

Statistical analysis

Normality of the data was assessed using the Shapiro-Wilk Test. Continuous data are presented as median (interquartile range, IQR), while categorical data is given as number (%). Differences between pre- and postoperatively obtained variables were tested with a paired samples *z*-test for parametric data and a Wilcoxon signed-rank test for non-parametric data. P values <0.05 were considered significant. Statistical analysis was performed using IBM SPSS statistics 26 (IBM corporation, Armonk, NY, USA).

Results

After visual inspection of all ECG-gated CTA scans of the fifteen patients, three patients were excluded for further analysis; one patient did not receive the dedicated IIA component, and two patients had insufficient CTA scans due to improper contrast distribution and retrospective gating (Figure 3). Patient-, aneurysm- and procedural characteristics of the remaining 12 patients (with a total of 14 devices) are depicted in Table I.[28]

Motion patterns

Both pre- and postoperatively the most prominent motion is observed in the *z*-direction (Figure 4), especially at the aorta- and CIA bifurcation (points 1-4). Motion decreased downstream the aorto-iliac tract in all directions. Points selected on opposite sides of the artery (or stent), *i.e.* points 1 and 2, 3 and 4, and 5 and 6, show similar motion patterns, hence little to no pulsatile expansion is observed. Motion amplitude increased significantly after IBE placement in the *y*-direction at the distal marker of the IIA component (point 5; P=0.024) and at the first IIA bifurcation (point 7; P=0.040). Moreover, a significant increase was found in the *z*-direction at the IBE flow divider (points 3 and 4; P=0.031, P=0.030) and the IIA bifurcation (point 7; P=0.001).

The pathlengths reflect similar results (Figure 5). Preoperatively, the pathlength reduced significantly from 2.4 mm (IQR 2.1, 3.0 mm) at the aorta bifurcation (point 1) to 1.6 mm (IQR 0.8, 1.7 mm; P=0.009) at the IIA bifurcation (point 7). Postoperatively, the pathlength decreased significantly as well, from 2.8 mm (IQR 2.2, 3.1 mm) at the bifurcation of the main endoprosthesis (point 1) to 1.7 mm (IQR 1.5, 2.0 mm; P=0.005) at the first IIA bifurcation (point 7). For each point the median pathlength increased

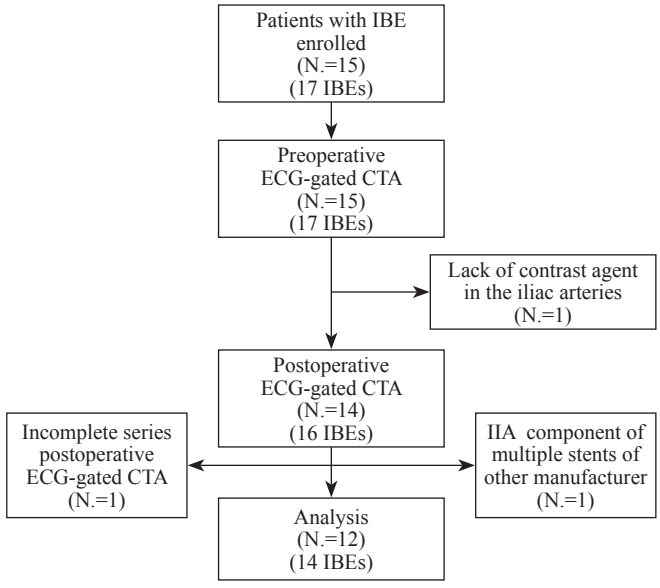

Figure 3.—Data inclusion flowchart.
IBE: iliac branch endoprosthesis; CTA: computed tomography angiography; ECG: electrocardiogram, IIA: internal iliac artery.

TABLE I.—*Patient-, aneurysm- and procedural characteristics.*

Patient characteristics	Values
Age, years	68.5 (64.3-74.5)*
Male sex	10 (83.3)
Cardiovascular risk factors (SVS grading system)[28]	Total (grade 0/1/2/3)
Diabetes	12 (100)/ - / - / -
Tobacco use	8 (66.7) / 2 (16.7) / 2 (16.7) / -
Hypertension	5 (41.7) / 3 (25) / 2 (16.7) / 2 (16.7)
Renal status	11 (91.7) / 1 (8.3) / - / -
Hyperlipidemia	5 (41.7) / - / - / 7 (58.3)
Cardiac status	10 (83.3) / 1 (8.3) / 1 (8.3) / -
Pulmonary status	11 (91.7) / 1 (8.3) / - / -
Aneurysm characteristics	
Infrarenal aneurysm	7 (58.3)
Aneurysm type (EUROSTAR A/B/C/D/E)	- / - / - / 12 (100) / -
CIA aneurysm (right/left/both/neither)	4 (33.3) / 5 (41.7) / 3 (25.0) / -
EIA aneurysm (right/left/both/neither)	- / - / - / 12 (100)
IIA aneurysm (right/left/both/neither)	2 (16.7) / 1 (8.3) / 1 (8.3) / 8 (66.7)
Vessel geometries, mm	
Diameter infrarenal aortic neck, mm	21.8 (20.0-24.9)*
Maximum diameter infrarenal aorta, mm	45.0 (26.1-59.1)*
Maximum diameter treated CIA, mm	36.6 (28.6-47.4)*
Length right CIA, mm	58.8 (47.2-73.3)*
Length left CIA, mm	51.7 (48.7-66.7)
Maximum diameter right IIA, mm	9.2 (7.3-16.3)
Maximum diameter left IIA, mm	9.6 (8.3-13.6)
Maximum diameter right EIA, mm	10.3 (9.6-12.3)*
Maximum diameter left EIA, mm	10.3 (8.7-12.0)*
Procedural characteristics	
Primary procedure (EVAR[#]+IBE/revision EVAR/IBE only)	8 (66.7) / 1 (8.3) / 3 (25.0)
Side of IBE (right/left/both)	5 (41.7) / 5 (41.7) / 2 (16.7)
Diameter IIA component, mm (7[Y]/8[Y]/10/12/13[Y]/14.5)	1 (8.3)[Y] / 1 (8.3)[Y] / 4 (33.3) / 3 (33.3) / 1 (8.3)[Y] / 4 (33.3)

Data presented as median (IQR), indicated with a * when normally distributed, or as number (%).
SVS: Society of Vascular Surgery; CIA: common iliac artery; EIA: external iliac artery; IIA: internal iliac artery; EVAR: endovascular aneurysm repair; IBE: iliac branch endoprosthesis.
[#]All EVAR grafts implanted in conjunction with an IBE were from the *GORE*® EXCLUDER® platform; [Y]Viabahn stents. Two patients received a self-expanding IIA component extended with a Viabahn, one patient received a Viabahn only.

after IBE placement, however, this increase was not statistical significant (P≥0.056).

The inter-observer variability for motion amplitudes was median 0.000 mm (-0.028 to 0.029 mm, ICC 0.839 P<0.01) and for pathlengths median 0.007 mm (IQR -0.044 – 0.093 mm, ICC 0.982 P<0.01); the intra-observer variability for motion amplitudes was median 0.001 (IQR -0.024 to 0.027, ICC 0.853 P<0.01) and for pathlengths median 0.007 mm (IQR -0.044 – 0.093 mm, ICC 0.982 P<0.01). These are all well within the previously established maximum error of amplitude calculation of 0.3 mm.[24]

Geometrical changes

Average and maximum static curvature of the native CIA-IIA trajectory were respectively 49.8 m^{-1} (IQR 43.2, 67.0) and 185.1 m^{-1} (IQR 144.0, 234.1), Figure 6. After treatment both average and maximum curvature significantly decreased to 35.3 m^{-1} (IQR 32.8, 40.6; P=0.006) and 122.5 m^{-1} (IQR 86.8, 167.9; P=0.012), respectively. Furthermore, the average dynamic curvature reduced from 2.2 m^{-1} (IQR 1.8, 2.6) to 1.6 m^{-1} (IQR 1.3, 1.9; P=0.005) and the maximum dynamic curvature from 7.6 m^{-1} (IQR 6.1, 8.6) to 4.9 m^{-1} (IQR 4.3, 6.1; P<0.001). Preoperatively, the maximum curvature was found at mid IIA in 3 out of 14 iliac trajectories, whereas postoperatively 9 out of 14 trajectories showed its maximum curvature at this location.

Average and maximum static torsion of the native CIA-IIA trajectory were respectively 190.0 m^{-1} (IQR 171.3, 207.4) and 2329.3 m^{-1} (IQR 1551.3, 3032.4), Figure 7. Neither showed a significant change after IBE implantation (P=0.573 and P=0.140, respectively). The average dynamic torsion increased significantly after IBE implantation from 30.7 m^{-1} (IQR 25.6, 34.8) to 38.2 m^{-1} (IQR 24.0, 77.2; P=0.037). The maximum dynamic torsion increased as well from 1303.7 (858.0, 1868.6) to 1841.0 (604.6, 4314.5), however not significant (P=0.079).

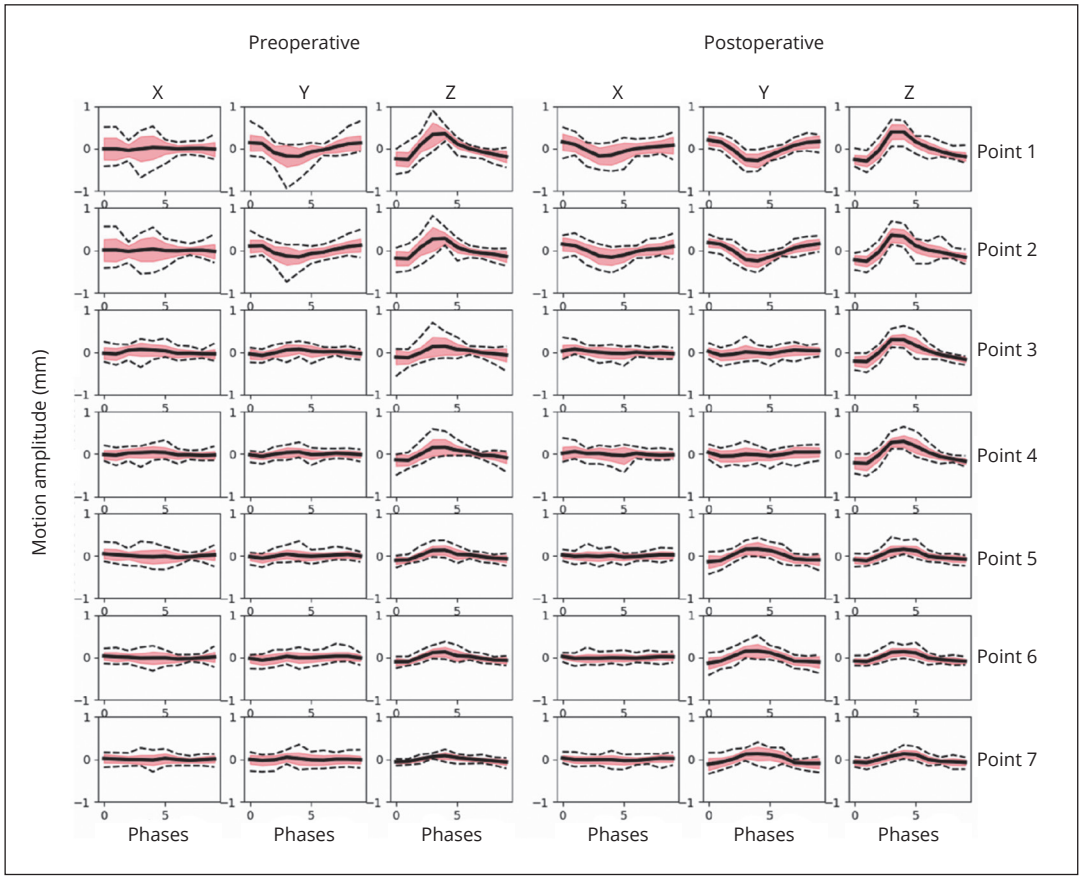

Figure 4.—Pre- and postoperative cardiac pulsatility-induced motion patterns per point. The motion amplitudes in *x*-, *y*- and *z*-direction are given as function of the 10 phases of the cardiac cycle. Motion amplitude decreases along the aorto-iliac tract. The solid black line represents the average motion amplitude, whereas the dashed black lines give the minimum and maximum value. The standard deviation is presented in pink.

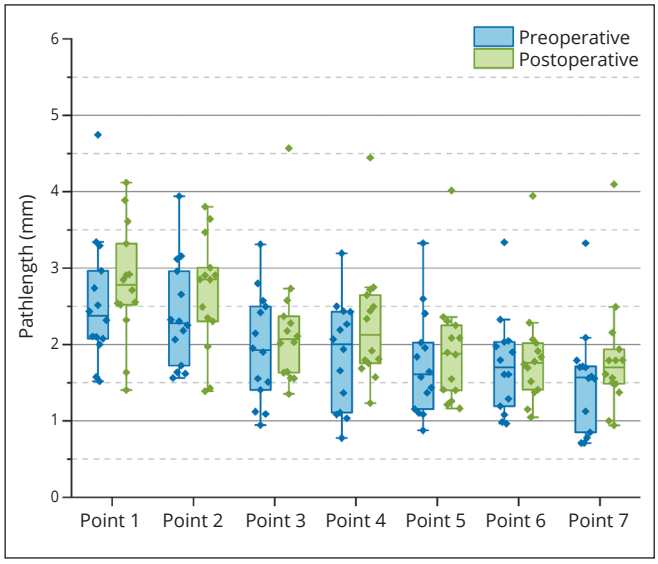

Figure 5.—Boxplots comparing pre- and postoperative pathlengths per point. Pathlengths decrease along the aorto-iliac tract. No significant differences were found between pre- and postoperative pathlengths.

The length of the native CIA-IIA trajectory was 170.5 mm (IQR 148.1, 206.5) and showed a variation of 0.9 mm (IQR 0.5, 1.1) during the cardiac cycle, Figure 8. Postoperatively, the length significantly decreased to 165.9 mm (IQR 139.6, 188.9; P=0.003) and its variation decreased to 0.6 mm (IQR 0.4, 0.7; P=0.035). The static TI reduced significantly from 1.28 (IQR 1.19, 1.30) to 1.18 (IQR 1.14, 1.23; P=0.002). The dynamic TI reduced significantly from 0.005 (IQR 0.004, 0.009) to 0.003 (IQR 0.002, 0.004; P=0.005).

Discussion

The present study performed detailed assessment of 3D cardiac pulsatility-induced motion patterns and geometrical changes of the CIA-IIA trajectory before and after IBE placement. Novel and in-depth analyses of ECG-gated CTA scans showed that after treatment with an IBE, motion increased especially at the distal end of the IIA component

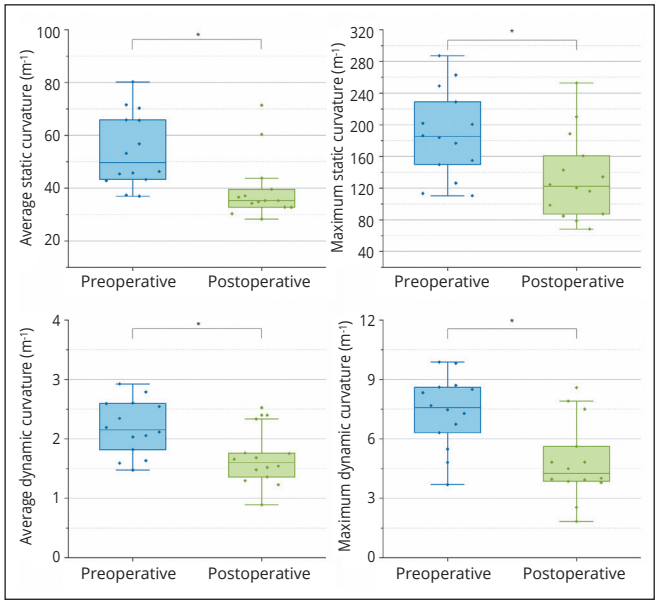

Figure 6.—Boxplots comparing pre- and postoperative static and dynamic curvature. The average and maximum curvature are presented.
*Significant differences.

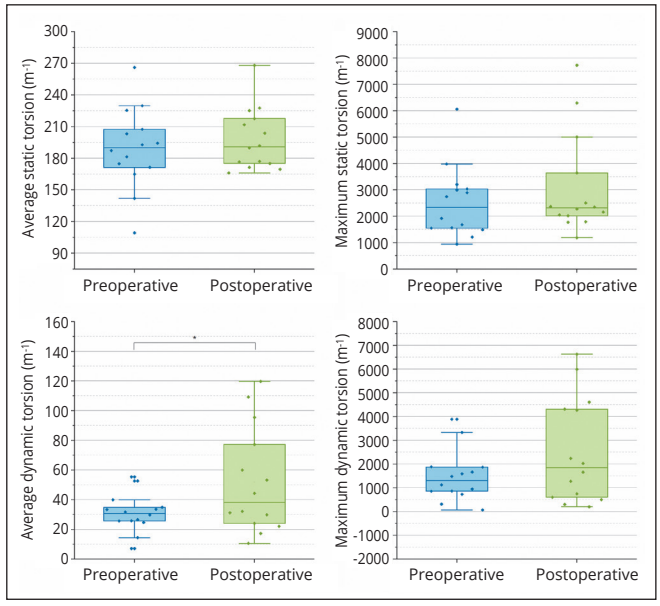

Figure 7.—Boxplots comparing pre- and postoperative static and dynamic torsion. The average and maximum torsion are presented.
*Significant differences.

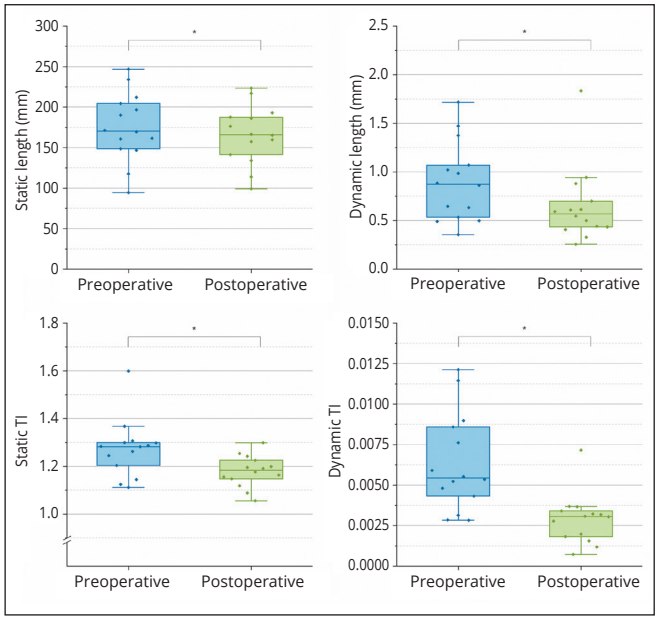

Figure 8.—Boxplots comparing pre- and postoperative static and dynamic length and tortuosity index (TI).
*Significant differences.

and the remnant native AII. This suggests less dampening of the cardiac pressure wave along the CIA-IIA trajectory and consequently increased forces on the IIA component, potentially challenging its durability.[29] In terms of geometrical changes, a significant decrease in both static and dynamic curvature, length and TI of the CIA-IIA trajectory was observed. This observation supports previous claims of stiffening, straightening and shortening of the aorto-iliac tract when treated with an endoprosthesis.[12, 17] The observed straightening and stiffening of the CIA-IIA trajectory in the current study is further supported by the relocation of the maximum curvature to the transition from distal IIA component and remnant IIA in nearly all patients. This implies that the stiffening of the stented vessel is somehow compensated at the transition between the IBE and the native IIA distal to the endoprosthesis. Consequently, hemodynamic and mechanical forces may be transferred from the IIA component to the native vessel, which might eventually cause injury to the intimal layer and may potentially promote thrombosis.[30]

While long-term clinical outcomes of the IBE are still awaited, midterm results reported by Schneider *et al.*[11] indicate a stable IIA component patency of 93.6% at both 6 and 24 months postoperatively and 91.8% remained free from reinterventions through 2 years. Five percent of patients experienced an occlusion of the IIA component within 1 month, suggesting that occlusion occurs due to anatomical, technical or geometrical factors. Out of the 12 patients analyzed, 1 patient presented with an occlusion of

the IIA component due to thrombus at the 6 weeks follow-up visit. Several differences compared to the remaining cohort were observed, namely a larger decrease in length, TI and curvature of the CIA-IIA trajectory after treatment. These findings might explain the early occlusion of the IIA component due to potential occurrence of flow disturbances, vessel damage and/or forces induced by the stiffness of the endoprosthesis. Consequently, patients with similar geometrical changes after graft placement might be at risk for occlusion. Nevertheless, the relation between clinical outcome and the dynamic and geometrical changes should be further investigated.

To the best of our knowledge conformability of the IBE is previously only addressed by Della Schiava *et al.*[17] who did not find significant differences in static length and TI of the CIA and CIA-EIA trajectory after treatment. Contrary to their results, significant differences in these parameters were found for the CIA-IIA trajectory in the present study which may be explained by the difference in study design. The dynamic behavior of the IIA or the IBE were not investigated by Della Schiava *et al.*[17] nor by other studies. Apfaltrer *et al.*[31] demonstrated that dynamic CTA is useful in endoleak detection after EVAR and Koenrades *et al.*[18] evaluated motion and deformation after endovascular aneurysm sealing with chimney grafts using ECG-gated CTA, while Ullery *et al.*[32] evaluated renal artery motion after fenestrated and snorkel/chimney EVAR on respiratory gated CTA.

Like in these previous studies, the current study underlines the main benefit of ECG-gated CT scanning: the ability to investigate dynamic behavior of vascular structures and endografts. However, a drawback of these types of CT scans is the extra radiation dose to which patients are exposed. By comparison, a standard CTA scan provide a radiation dose of about 4.6 mSv to a patient, while the ECG-gated CTA scans radiation dose is about 11 mSv. Based on a the ICRP 103 publication, the radiation exposure of 11 mSv (*i.e.* 1 ECG-gated CT) induces a lifetime attribute risk of all cancer of approximately 0.04% in adults. Considering the included population in the present study, *i.e.* mostly patients with comorbidities >65 years old, this risk might even be lower.

The investigated parameters gave insight in the geometry changes induced by IBE. Pre- to postoperative decrease in length may suggest compression and, when in combination with decreased TI and/or curvature, straightening of the vascular segment.[33] TI and curvature give insight in the curving of a vascular trajectory, based on the centerline. However, TI a general presentation of the experienced curves, while curvature can give more in depth insights into where the bending is most severe. Moreover, both parameters have been linked to (different) complications after EVAR.[15-17, 34, 35] For example, Dowson *et al.*[34] found that calculating TI over centerline segments of 10 mm aids to predict the likely success of EVAR and Spinella *et al.*[36] used curvature to evaluate the adaptability of a Viabahn balloon expandable stent graft in an IIA. Although curvature is increasingly accepted as a metric in characterizing vasculature and believed to be more accurate than angulation,[37] to fully describe the trajectory of a centerline in 3D, torsion should be considered as well.[27] However, literature in vascular research using torsion is scarce. This study showed an increase in the average dynamic torsion during the cardiac cycle. This may suggest an enhanced torsion during the cardiac cycle as compensation for the decreased curvature and stiffening. Despite being an important addition, caution should be taken with this variable considering its sensitivity to slight centerline inaccuracies and the clinical interpretation of static and dynamic torsion remains to be elucidated.

Limitations of the study

The study is limited by a relatively small sample size. Unfortunately, 2 patients in the present study had to be excluded due to insufficient ECG-gated CT scans. The first patient was excluded due to lack of contrast agent in the iliac arteries on the preoperative scan, probably caused by a combination of insufficient triggering and a large volume of the iliac aneurysm sac. The second patient was excluded because of incorrect retrospective gating and subsequent reconstruction of the 10 cardiac phases volumes of the postoperative scan. Unfortunately, the raw CT data was no longer available when this issue was discovered. Nevertheless, statistically significant changes were observed. Considering the prospective study design, in depth analysis of the ECG-gated CT scans and low observer variability in the measurements, these results can be considered reliable. Since this study only included patients treated with an IBE, the current data may not be generalized for all iliac branched devices. The algorithm used to assess motion has an error threshold of at most 0.3 mm.[38] Some of the observed motion patterns are close to or below this threshold and can therefore not be considered completely valid.

Conclusions

Treatment of an aorto-iliac aneurysm using an IBE to preserve blood flow through the IIA changes the dynamic and

static behavior of the treated trajectory, based on evaluation with dedicated ECG-gated CTA analysis algorithms. The IBE causes less dampening of the cardiac pressure wave and more motion of the IIA trajectory. Shortening and straightening of the CIA-IIA trajectory was reflected by the reduction in static curvature, length and TI. Furthermore, the curvature varied less during the cardiac cycle, indicating a stiffened trajectory. Whether these observations relate to loss of long-term integrity and patency of the IIA component remains to be elucidated.

References

1. Hinchliffe RJ, Alric P, Rose D, Owen V, Davidson IR, Armon MP, *et al.* Comparison of morphologic features of intact and ruptured aneurysms of infrarenal abdominal aorta. J Vasc Surg 2003;38:88–92.

2. Columbo JA, Martinez-Camblor P, O'Malley AJ, Suckow BD, Hoel AW, Stone DH, *et al.*; Society for Vascular Surgery's Vascular Quality Initiative. Long-term Reintervention After Endovascular Abdominal Aortic Aneurysm Repair. Ann Surg 2021;274:179–85.

3. Bastos Gonçalves F, Oliveira NF, Josee van Rijn M, Ultee KH, Hoeks SE, Ten Raa S, *et al.* Iliac Seal Zone Dynamics and Clinical Consequences After Endovascular Aneurysm Repair. Eur J Vasc Endovasc Surg 2017;53:185–92.

4. Criado FJ, Wilson EP, Velazquez OC, Carpenter JP, Barker C, Wellons E, *et al.* Safety of coil embolization of the internal iliac artery in endovascular grafting of abdominal aortic aneurysms. J Vasc Surg 2000;32:684–8.

5. Bosanquet DC, Wilcox C, Whitehurst L, Cox A, Williams IM, Twine CP; British Society of Endovascular therapy (BSET). Systematic Review and Meta-analysis of the Effect of Internal Iliac Artery Exclusion for Patients Undergoing EVAR. Eur J Vasc Endovasc Surg 2017;53:534–48.

6. Kouvelos GN, Katsargyris A, Antoniou GA, Oikonomou K, Verhoeven EL. Outcome after Interruption or Preservation of Internal Iliac Artery Flow During Endovascular Repair of Abdominal Aorto-iliac Aneurysms. Eur J Vasc Endovasc Surg 2016;52:621–34.

7. van Sterkenburg SM, Heyligers JM, van Bladel M, Verhagen HJ, Eefting D, van Sambeek MR, *et al.*; Dutch IBE Collaboration. Experience with the GORE EXCLUDER iliac branch endoprosthesis for common iliac artery aneurysms. J Vasc Surg 2016;63:1451–7.

8. Schneider DB, Matsumura JS, Lee JT, Peterson BG, Chaer RA, Oderich GS. Prospective, multicenter study of endovascular repair of aortoiliac and iliac aneurysms using the Gore Iliac Branch Endoprosthesis. J Vasc Surg 2017;66:775–85.

9. Millon A, Della Schiava N, Arsicot M, De Lambert A, Feugier P, Magne JL, *et al.* Preliminary Experience with the GORE(®) EXCLUDER(®) Iliac Branch Endoprosthesis for Common Iliac Aneurysm Endovascular Treatment. Ann Vasc Surg 2016;33:11–7.

10. Ferrer C, De Crescenzo F, Coscarella C, Cao P. Early experience with the Excluder® iliac branch endoprosthesis. J Cardiovasc Surg (Torino) 2014;55:679–83.

11. Schneider DB, Milner R, Heyligers JM, Chakfé N, Matsumura J. Outcomes of the GORE Iliac Branch Endoprosthesis in clinical trial and real-world registry settings. J Vasc Surg 2019;69:367–377.e1.

12. Lee K, Leci E, Forbes T, Dubois L, DeRose G, Power A. Endograft conformability and aortoiliac tortuosity in endovascular abdominal aortic aneurysm repair. J Endovasc Ther 2014;21:728–34.

13. Coulston J, Baigent A, Selvachandran H, Jones S, Torella F, Fisher R. The impact of endovascular aneurysm repair on aortoiliac tortuosity and its use as a predictor of iliac limb complications. J Vasc Surg 2014;60:585–9.

14. Taudorf M, Jensen LP, Vogt KC, Grønvall J, Schroeder TV, Lönn L. Endograft limb occlusion in EVAR: iliac tortuosity quantified by three different indices on the basis of preoperative CTA. Eur J Vasc Endovasc Surg 2014;48:527–33.

15. Wyss TR, Dick F, Brown LC, Greenhalgh RM. The influence of thrombus, calcification, angulation, and tortuosity of attachment sites on the time to the first graft-related complication after endovascular aneurysm repair. J Vasc Surg 2011;54:965–71.

16. Simmering JA, Geelkerken RH, Slump CH, Koenrades MA. Geometrical changes in Anaconda endograft limbs after endovascular aneurysm repair: A potential predictor for limb occlusion. Semin Vasc Surg 2020;32:94–105.

17. Della Schiava N, Arsicot M, Boudjelit T, Feugier P, Lermusiaux P, Millon A. Conformability of GORE Excluder Iliac Branch Endoprosthesis and COOK Zenith Bifurcated Iliac Side Branched Iliac Stent Grafts. Ann Vasc Surg 2016;36:139–44.

18. Koenrades MA, Donselaar EJ, van Erp MA, Loonen TG, van Lochem P, Klein A, *et al.* Electrocardiography-gated computed tomography angiography analysis of cardiac pulsatility-induced motion and deformation after endovascular aneurysm sealing with chimney grafts. J Vasc Surg 2020;72:1743–1752.e5.

19. van Keulen JW, Moll FL, Barwegen GK, Vonken EP, van Herwaarden JA. Pulsatile distension of the proximal aneurysm neck is larger in patients with stent graft migration. Eur J Vasc Endovasc Surg 2010;40:326–31.

20. Teutelink A, Muhs BE, Vincken KL, Bartels LW, Cornelissen SA, van Herwaarden JA, *et al.* Use of dynamic computed tomography to evaluate pre- and postoperative aortic changes in AAA patients undergoing endovascular aneurysm repair. J Endovasc Ther 2007;14:44–9.

21. Muhs BE, Vincken KL, Teutelink A, Verhoeven EL, Prokop M, Moll FL, *et al.* Dynamic cine-computed tomography angiography imaging of standard and fenestrated endografts: differing effects on renal artery motion. Vasc Endovascular Surg 2008;42:25–31.

22. van Keulen JW, Vincken KL, van Prehn J, Tolenaar JL, Bartels LW, Viergever MA, *et al.* The influence of different types of stent grafts on aneurysm neck dynamics after endovascular aneurysm repair. Eur J Vasc Endovasc Surg 2010;39:193–9.

23. Itoga NK, Suh GY, Cheng CP. Stabilization of the Abdominal Aorta During the Cardiac Cycle with the Sac-Anchoring Nellix Device. Ann Vasc Surg 2018;52:312.e7–12.

24. Koenrades MA, Struijs EM, Klein A, Kuipers H, Reijnen MM, Slump CH, *et al.* Quantitative Stent Graft Motion in ECG Gated CT by Image Registration and Segmentation: In Vitro Validation and Preliminary Clinical Results. Eur J Vasc Endovasc Surg 2019;58:746–55.

25. Klein A, Jan Renema WK. der Vliet JA van, J.Oostveen L, Hoogeveen Y, Schultze Kool LJ, *et al.* Motion Calculations on Stent Grafts in AAA. In: Grundmann RT, editor. Diagnosis, Screening and Treatment of Abdominal, Thoracoabdominal and Thoracic Aortic Aneurysms. Rijeka, Croatia: InTechOpen; 2011. pp. 125–44.

26. Klein A, van der Vliet JA, Oostveen LJ, Hoogeveen Y, Kool LJ, Renema WK, *et al.* Automatic segmentation of the wire frame of stent grafts from CT data. Med Image Anal 2012;16:127–39.

27. O'Flynn PM, O'Sullivan G, Pandit AS. Geometric variability of the abdominal aorta and its major peripheral branches. Ann Biomed Eng 2010;38:824–40.

28. Stoner MC, Calligaro KD, Chaer RA, Dietzek AM, Farber A, Guzman RJ, *et al.*; Society for Vascular Surgery. Reporting standards of the Society for Vascular Surgery for endovascular treatment of chronic lower extremity peripheral artery disease. J Vasc Surg 2016;64:e1–21.

29. Jacobs TS, Won J, Gravereaux EC, Faries PL, Morrissey N, Teodorescu VJ, *et al.* Mechanical failure of prosthetic human implants: a 10-year experience with aortic stent graft devices. J Vasc Surg 2003;37:16–26.

30. Blann AD. How a damaged blood vessel wall contibutes to thrombosis and hypertenasion. Pathophysiol Haemost Thromb 2003;33:445–8.

31. Apfaltrer G, Lavra F, Schoepf UJ, Scarabello M, Yamada R, van As-

sen M, *et al.* Quantitative analysis of dynamic computed tomography angiography for the detection of endoleaks after abdominal aorta aneurysm endovascular repair: A feasibility study. PLoS One 2021;16:e0245134.

32. Ullery BW, Suh GY, Kim JJ, Lee JT, Dalman RL, Cheng CP. Dynamic Geometric Analysis of the Renal Arteries and Aorta following Complex Endovascular Aneurysm Repair. Ann Vasc Surg 2017;43:85–95.

33. Lee K, Hossain S, Sabalbal M, Dubois L, Duncan A, DeRose G, *et al.* Explaining endograft shortening during endovascular repair of abdominal aortic aneurysms in severe aortoiliac tortuosity. J Vasc Surg 2017;65:1297–304.

34. Dowson N, Boult M, Cowled P, De Loryn T, Fitridge R. Development of an automated measure of iliac artery tortuosity that successfully predicts early graft-related complications associated with endovascular aneurysm repair. Eur J Vasc Endovasc Surg 2014;48:153–60.

35. Schuurmann RC, Ouriel K, Muhs BE, Jordan WD Jr, Ouriel RL, Boersen JT, *et al.* Aortic curvature as a predictor of intraoperative type Ia endoleak. J Vasc Surg 2016;63:596–602.

36. Spinella G, Mambrini S, Finotello A, Conti M, Del Pizzo R, Pratesi G, *et al.* Endovascular Treatment of an Internal Iliac Artery Aneurysm in a Patient with Previous Aortic Surgery Using a Novel Covered Stent Graft. Ann Vasc Surg 2020;64:412.e15–9.

37. Schuurmann RC, Kuster L, Slump CH, Vahl A, van den Heuvel DA, Ouriel K, *et al.* Aortic curvature instead of angulation allows improved estimation of the true aorto-iliac trajectory. Eur J Vasc Endovasc Surg 2016;51:216–24.

38. Koenrades MA, Struijs EM, Klein A, Kuipers H, Geelkerken RH, Slump CH. Validation of an image registration and segmentation method to measure stent graft motion on ECG-gated CT using a physical dynamic stent graft model. Med Imaging 2017 Comput Diagnosis 2017;10134:1013418.

Conflicts of interest.—Michel M.P.J. Reijnen is a consultant for Gore Med. All other authors have no conflicts of interest to declare.

Funding.—This work was funded by unrestricted grants from Gore Medical and by the PPP Allowance made available by Health~Holland, Top Sector Life Sciences & Health.

Authors' contributions.—Majorie van Helvert and Jaimy A. Simmering contributed equally to this work and have shared first authorship. All authors read and approved the final version of the manuscript.

History.—Article first published online: January 10, 2022. - Manuscript accepted: January 5, 2022. - Manuscript revised: October 18, 2021. - Manuscript received: June 1, 2021.